03

Convection of a stratified ferrofluid in a modulated magnetic field

© P.N. Kazantsev, B.L. Smorodin

Perm State University,
614990 Perm, Russia
e-mail: kazantsevpn@yandex.ru

Received July 16, 2025
Revised October 6, 2025
Accepted October 19, 2025

The paper studies the convective stability of the stratified by magnetophoresis and thermal diffusion ferrofluid, placed in a heated from its narrow face Hele–Shaw cell. The cell is subjected to a nonuniform magnetic field with a modulated contribution. The characteristics of parametric instability are obtained, and depicted in the graphs of the dependence of critical magnetic Rayleigh numbers on the amplitude and inverse frequency of external modulation. The types of emerging flows are described and their evolution over time is presented.

Keywords: ferrofluid, magnetophoresis, thermal diffusion, Hele-Shaw cell, parametric resonance.

DOI: 10.61011/TP.2026.02.62874.186-25

Introduction

Ferrofluids (FF) are colloidal solutions of magnetic nanoparticles in a non-magnetic carrier fluid [1–3]. In certain conditions, FF behave as uniformly graded fluids, whose magnetization $M(T)$ depends on temperature T. Under the action of magnetic field gradient (external or induced), colder FF elements are exposed to a high Kelvin force $\mathbf{F_k} = M\nabla H$ (H — magnetic field strength) pulling them into a strong field region and causing the flow. Large body of literature is devoted to this phenomenon known as the thermomagnetic convection [4–7].

There is another class of phenomena, which can be only explained by assuming that FF is nonuniformly graded fluid, whose volume fraction of magnetic particles $\varphi(\mathbf{r}, t)$ varies with time and space. Increase in nonuniformity can be caused by various magnetic nanoparticle transport mechanisms: magnetophoresis and thermodiffusion [8–10]. On the other hand, diffusion and convective stirring „smooth" nonuniformities. In this case, convection can occur in an oscillatory manner: neutral oscillations at the instability threshold are characterized by an natural frequency ω_0. Nonlinear oscillatory modes are generated in the course of evolution.

Behavior of mechanical and, in particular, hydrodynamic systems having natural oscillation frequency in alternating external fields of different origin (vibrational [11,12], thermal, electric [13,14], magnetic [9]) demonstrates a parametric resonance phenomenon [15,16].

Variable action provides heat exchange control via switching between flow modes having various intensities and, consequently, heat transfer, and also provides full convection suppression.

This work describes the action of a variable magnetic field on stability thresholds, incremental disturbance behavior and nonlinear FF in the Hele–Shaw cell.

1. Problem formulation

Consider the Hele–Shaw cell [17]. Spacing between wide faces of the cell ($2d$) is much smaller than height $h = 20d$ and length $l = 40d$ of the cell. The cell is filled with FF (colloidal suspension) with viscosity η, thermal diffusivity κ and magnetic susceptibility χ (Figure 1) and is placed in the external inhomogeneous constant magnetic field generated by two magnets in the form of rings (Figure 2, *3*). Since the cell with FF is well centered between the ring magnets and its height is small compared with the distance between the rings $2z_0 = 3.4R$, the field in the cell is characterized by a linear dependence [9,18]:

$$\mathbf{H}_c = (0, 0, Gz), \quad G = 0.244K/R^3,$$

where $K = 4\pi M_r \mathcal{L}(R_2 - R_1)$ is the parameter depending on magnetization M_r, thickness $\mathcal{L}$ and inside radius R_1 and outside radius R_2 of the magnet rings, $R = (R_2 + R_1)/2$ is

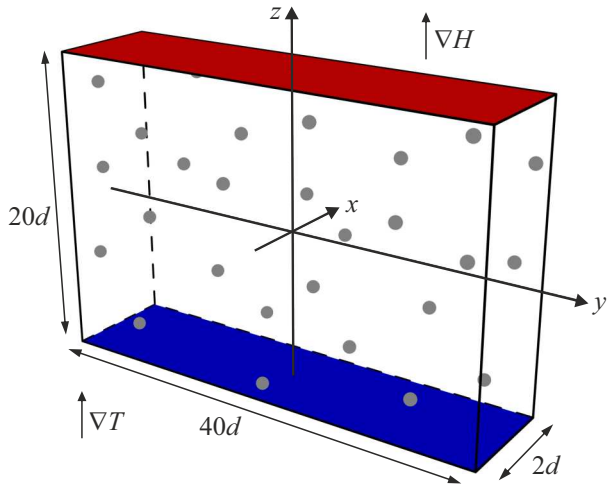

Figure 1. Hele–Shaw cell.

the mean ring radius. Note that external magnetic field strength $\mathbf{H}_c$ is an odd function of the z coordinate: its projection of the z axis is negative with $z < 0$ (Figure 2).

Besides the constant field of ring magnets $\mathbf{H}_c$, the ferrofluid is exposed to the alternating magnetic field $\mathbf{H}_a$ with an amplitude A and frequency ω_* generated by the Helmholtz coils placed on both sides of the cell (Figure 2, *3*):

$$\mathbf{H}_a = (0, 0, A\cos\omega_* t).$$

Cell faces perpendicular to the magnetic field gradient (Figure 1) are maintained at different constant temperatures forming the difference ΔT, so the cell has a temperature gradient co-directional with the field strength gradient. Faces perpendicular to the x axis (wide faces) are heat insulated. FF behavior is considered in zero-gravity state — gravity is absent.

The system of FF convection equations contains the Navier–Stokes equation, including the Kelvin magnetic force, continuity equation for incompressible fluid, thermal conductivity equation, and equation for evolution of the volume fraction $\varphi(\mathbf{r}, t)$ of magnetic particles [4,9,19]:

$$\rho\left(\frac{\partial \mathbf{v}}{\partial t} + (\mathbf{v}\cdot\nabla)\mathbf{v}\right) = -\nabla p + \eta\Delta\mathbf{v} + M\nabla H, \quad \nabla\cdot\mathbf{v} = 0, \tag{1}$$

$$\frac{\partial T}{\partial t} + (\mathbf{v}\cdot\nabla)T = \kappa\Delta T, \tag{2}$$

$$\frac{\partial \varphi}{\partial t} + (\mathbf{v}\cdot\nabla)\varphi + \mathrm{div}\,\mathbf{j} = 0, \tag{3}$$

$$\mathbf{j} = \varphi\mathbf{u} - D\left(\nabla\varphi + \mathrm{S_T}\nabla T\right), \quad 3\pi\eta a\,\mathbf{u} = \frac{m^2 H}{3k_B T_*}\nabla H, \tag{4}$$

where ρ is the fluid density, $\mathbf{v}$ is the velocity, p is the pressure, η is the shear-viscosity coefficient, κ is the thermal diffusivity coefficient, T is the temperature, $\boldsymbol{j}$ is the density of magnetic particle flux, $D = k_B T_*/3\pi\eta a$ is the diffusion constant of nanoparticles with the diameter a, k_B is the Boltzmann constant, $\mathrm{S_T}$ is the Soret coefficient, $\mathbf{u}$ is the velocity of particles with respect to the carrier fluid induced by the magnetic force, T_* is the mean temperature in mechanical equilibrium state, m is the magnetic moment of colloidal particle.

Due to heavy nonuniformity of the external magnetic field, its deviations in the real FF cell from the external distribution $H = Gz + A\cos\omega_* t$ can be considered as insignificant [9]. Thus, the Maxwell equations may be not included in system (1)–(4).

At the horizontal boundaries of the cell, no-slip conditions shall be satisfied for the velocity, temperature constancy and impermeability for magnetic particles:

$$z = \ \ h/2: \ T = T_* + \Delta T/2, \ \mathbf{v} = 0, \ \mathbf{j} = 0,$$

$$z = -h/2: \ T = T_* - \Delta T/2, \ \mathbf{v} = 0, \ \mathbf{j} = 0.$$

Fluid magnetization is Langevinian and, due to smallness of the magnetic field within the layer [9], depends linearly on the strength:

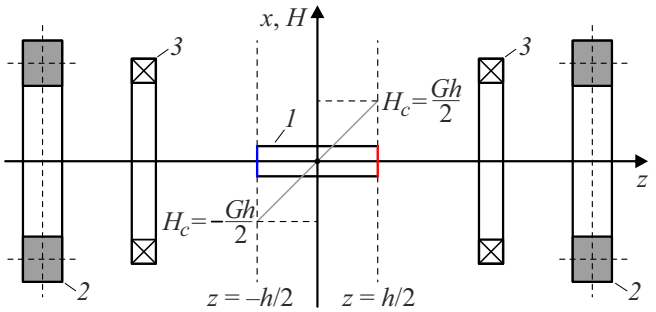

Figure 2. Position of the Hele–Shaw cell (*1*) with respect to the ring magnets (*2*) and Helmholtz coils (*3*).

$$M = \chi(\varphi, T)\,H, \qquad \chi = \frac{\varphi M_s m}{3k_B T},$$

where M_s is the saturation magnetization of the dispersed ferromagnetic.

If ΔT lower than critical differential temperature is applied to the cell, FF will be in the state of rest ($\mathbf{v} = 0$). With mechanical equilibrium, the temperature distribution according to (2) is written as

$$T_0 = T_* + \frac{\Delta T}{h}z.$$

Being in such state for a long time, FF can be stratified under the action of inhomogeneous temperature and magnetic fields. Thus, substituting $\mathbf{j} = 0$ into equation (4), we get the equilibrium concentration distribution — a parabolic profile induced by magnetophoresis [9], which shifts vertically under the action of thermodiffusion [10]:

$$\varphi_0 = \left(1 + \frac{\gamma^2\left(12\,(z/h)^2 - 1\right)}{72}\right)\overline{\varphi} - \mathrm{S_T}\Delta T\frac{z}{h},$$

$$\gamma = \frac{mGh}{k_B T}, \tag{5}$$

where $\overline{\varphi}$ is the mean concentration of magnetic particles.

Since the magnetophoresis acts only in an inhomogeneous magnetic field, the time-varying additive provided by the ring magnets will not affect the redistribution of magnetic particles. On the other hand, this magnetic field component is the source of parametric impact on FF.

Note that expression (5) was derived for $\gamma^2 \ll 1$ corresponding to experimental cases (for example, $\gamma^2 = 0.25$ [9]).

2. Plane flows in the Hele–Shaw cell

In plane trajectory approximation ($v_x = 0$) [20], which is true in the case when the cell width and length are much larger than the gap between the wide faces

($l \gg 2d, h \gg 2d$), it is convenient to introduce the flow function

$$v_y = -\frac{\partial \Psi}{\partial z}, v_z = \frac{\partial \Psi}{\partial y},$$

and vorticity

$$\Phi = [\mathrm{rot}\,\mathbf{v}]_x .$$

Solution to the system is written as

$$\mathbf{v} = \left[0,\ -\frac{\partial \Psi}{\partial z},\ \frac{\partial \Psi}{\partial y}\right] \cos\left(\frac{\pi x}{2}\right),$$

$$T = T_0(z) + T'(t, y, z),$$

$$\varphi = \varphi_0(z) + \varphi'(t, y, z),$$

as in the case of thermal convection of the colloidal suspension in the Hele–Shaw cell in the constant field [10].

Independence of functions for temperature and concentration from the transverse x coordinate corresponds to the case of heat insulated wide faces, on which there is no magnetic nanoparticle flux.

We choose the following units of measurement: distance — cell half-thickness d, time — $\frac{d^2}{\kappa}$, velocity — $\frac{\kappa}{d}$, temperature — $T_* \frac{\eta\kappa}{\chi_* G^2 d^4}$, concentration — $\overline{\varphi} \frac{\eta\kappa}{\chi_* G^2 d^4}$.

After averaging of equations (1)–(3) across the cell, the dimensionless system of equations with respect to Ψ and deviations of temperature $T' = T - T_0$ and concentration $\varphi' = \varphi - \varphi_0$ from their equilibrium values is written as:

$$\frac{\partial \Phi}{\partial t} + \frac{8}{3\pi}\left[\frac{\partial \Psi}{\partial y}\frac{\partial \Phi}{\partial z} - \frac{\partial \Psi}{\partial z}\frac{\partial \Phi}{\partial y}\right] = Pr\left[\Delta_\perp \Phi - \frac{\pi^2}{4}\Phi + \frac{4}{\pi}(z + \xi\cos\omega t)\left(\frac{\partial \varphi'}{\partial y} - \frac{\partial T'}{\partial y}\right)\right],$$

$$\frac{\partial T'}{\partial t} + \frac{2}{\pi}\left[\frac{\partial \Psi}{\partial y}\frac{\partial T'}{\partial z} - \frac{\partial \Psi}{\partial z}\frac{\partial T'}{\partial y}\right] = \Delta_\perp T' - \frac{2}{\pi} R_m \frac{\partial \Psi}{\partial y},$$

$$\Phi = \Delta_\perp \Psi, \qquad (6)$$

$$\frac{\partial \varphi'}{\partial t} + \frac{2}{\pi}\left[\frac{\partial \Psi}{\partial y}\frac{\partial \varphi'}{\partial z} - \frac{\partial \Psi}{\partial z}\frac{\partial \varphi'}{\partial y}\right] = Le\left[\Delta_\perp \varphi' + \psi \Delta_\perp T' - \frac{\gamma^2}{3}\left(z\frac{\partial \varphi'}{\partial z} + \varphi'\right)\right] - \frac{2}{\pi}(R_c z - R_m \psi)\frac{\partial \Psi}{\partial y},$$

where $\Delta_\perp = \frac{\partial^2}{\partial y^2} + \frac{\partial^2}{\partial z^2}$, and also dimensionless parameters are used $Pr = \eta/\rho\kappa$ — Prandtl number, $\xi = A/Gd$ and $\omega = \omega_* d^2/\kappa$ — dimensionless amplitude and modulation frequency of the external magnetic field, $R_m = \frac{\Delta T}{T_*}\frac{\chi_* G^2 d^4}{\kappa\eta}$ — Rayleigh magnetic number, $R_c = \frac{\gamma^2}{3}\frac{\chi_* G^2 d^4}{\kappa\eta}$ — Rayleigh concentration number, $\chi_* = \frac{\overline{\varphi} M_s m}{3 k_B T_*}$ — magnetic susceptibility with mean equilibrium temperature and concentration, $Le = D/\kappa$ — Lewis number, $\psi = S_T T_*/\overline{\varphi}$ — mixture separation coefficient characterizing thermodiffusion separation.

In the mechanical equilibrium state, temperature and concentration gradients are written as:

$$\frac{dT_0}{dz} = R_m, \quad \frac{d\varphi_0}{dz} = R_c z - R_m \psi.$$

dimensionless parameters R_c and ψ characterize the initial degree of FF nonuniformity induced by magnetophoresis and thermophoresis, respectively.

The following conditions shall be satisfied at the cell boundaries:

$$y = \pm 20: \quad \Psi = \frac{\partial^2 \Psi}{\partial y^2} = \frac{\partial T'}{\partial y} = \frac{\partial \varphi'}{\partial y} = 0, \qquad (7)$$

$$z = \pm 10: \quad \Psi = \frac{\partial^2 \Psi}{\partial z^2} = T' = \varphi' = 0. \qquad (8)$$

3. Galerkin procedure

We use the Galerkin procedure to study the FF flow evolution under the action of alternating field [20,21]. We seek an approximate solution to the problem in the form of superposition of the basis functions (space harmonics) satisfying the boundary conditions (7), (8):

$$\Psi = \sum_{n,m=1}^{n_{\max}, m_{\max}} \Psi_{nm}(t)\mathrm{CS}\left(\frac{n\pi y}{40}\right)\mathrm{CS}\left(\frac{m\pi z}{20}\right),$$

$$T' = \sum_{n=0,m=1}^{n_{\max}, m_{\max}} \theta_{nm}(t)\mathrm{SC}\left(\frac{n\pi y}{40}\right)\mathrm{CS}\left(\frac{m\pi z}{20}\right),$$

$$\varphi' = \sum_{n=0,m=1}^{n_{\max}, m_{\max}} \varphi_{nm}(t)\mathrm{SC}\left(\frac{n\pi y}{40}\right)\mathrm{CS}\left(\frac{m\pi z}{20}\right),$$

where

$$\mathrm{CS}(nx) \equiv \left\{ \begin{array}{ll} \cos nx, & \text{odd } n \\ \sin nx, & \text{even } n \end{array} \right\},$$

$$\mathrm{SC}(nx) \equiv \left\{ \begin{array}{ll} \sin nx, & \text{odd } n \\ \cos nx, & \text{even } n \end{array} \right\}.$$

Expansion coefficients $\Psi_{nm}(t)$, $\theta_{nm}(t)$, $\varphi_{nm}(t)$ are determined from integral conditions expressing the residual orthogonality to each basis function. After applying the Galerkin procedure at $n_{\max} = 6$ and $m_{\max} = 2$, a system of 40 nonlinear equations with respect to tine-dependent general amplitudes $X_i(t) = (\Psi_{nm}(t),\ \theta_{nm}(t),\ \varphi_{nm}(t))$ was derived:

$$\dot{X}_i = \sum_j a_{ij} X_j + \sum_{jk} b_{ijk} X_j X_k.$$

Thus, the partial differentiation problem is reduced to solution of a simpler system of ordinary differential equations for the expansion coefficients, which was later solved using the numerical integration by the Runge–Kutta–Fehlberg method of the 4–5th order of accuracy in „Maple“ computer

algebra system. As initial conditions for velocity, and for temperature and concentration deviations, amplitudes were set to 0.01 and to 0, respectively.

To find parametric instability thresholds, Floquet theory was used [22], according to which

$$X(t) = e^{\lambda t} X_*(t), \quad X_*(t) = \begin{pmatrix} \Psi_{nm} \\ \theta_{nm} \\ \varphi_{nm} \end{pmatrix},$$

where $X(t)$ and $X_*(t)$ — are vector functions of dimension 40, $X_*(t)$ is time-periodic with the period $\tau = 2\pi/\omega$, $e^{\lambda t}$ is the Floquet multiplier and $\lambda = \lambda_r + i\lambda_i$ is the complex growth exponent.

Using the suitable initial conditions, we get K linearly independent solutions for coefficients $(\Psi_{nm}(t), \theta_{nm}(t), \varphi_{nm}(t))$ at the and of one modulation period τ. These fundamental solutions are K columns of monodromy matrix $K \times K$. The Cauchy problem is solved using the fourth order Runge-Kutta method. Eigenvalues of the monodromy matrix are a set of Floquet multipliers $\gamma_k = e^{\lambda_k \tau}$. Eigenvalues γ_k were derived using the QR algorithm [23]. Time-periodic solution describing the equilibrium is stable when the absolute value of any multiplier $|\gamma_k|$ is not larger than 1. In case when multipliers are ordered, the sequence of inequalities $1 \geq |\gamma_1| \geq \cdots \geq |\gamma_k|$ is satisfied. For the instability boundary, we have condition $|\gamma_1| = 1$, which defines neutral variety in the space of parameters R_m, R_c, Pr and ψ. $\gamma_1 = -1$ corresponds to $\lambda_r = 0, \lambda_i = \omega/2$, i.e. neutral disturbances have a period which is twice as large as the external field period. These solutions correspond to a subharmonic response to the external field. When $\gamma_1 = 1 (\lambda_r = 0, \lambda_i = \omega)$, neutral disturbance period coincides with the excitation period — synchronous response. If instability occurs in the presence of pairs of complex conjugate eigenvalues with a single absolute value $|\gamma_1| = 1 (\lambda_r = 0, \lambda_i \neq \omega)$, then neutral disturbances are quasiperiodic with two different characteristic frequencies, which are not connected by a rational relation.

4. Parametric instability boundaries and supercritical flows

Linear analysis provided dependences of the critical magnetic Rayleigh number R_m^* characterizing the parametric convective instability threshold on amplitude ξ and magnetic field modulation frequency ω. A set of parameters typical of FF was used: $Pr = 10$, $Le = 10^{-4}$. It was assumed that the fluid was initially stratified owing to magnetophoresis $R_c = 0.9$ and thermodiffusion $\psi = 6$.

Figure 3 shows a curve of the threshold magnetic Rayleigh number R_m^* vs. the reduced inverse frequency of alternating magnetic field ω_0/ω, where $\omega_0 = 0.1238$ is the natural oscillation frequency of FF at the instability boundary in the constant magnetic field case ($\xi = 0$) [10]. For convenience, R_m^* was normalized to the maximum value in the region of the curve $R_{\max}^* = 0.495$. Red line

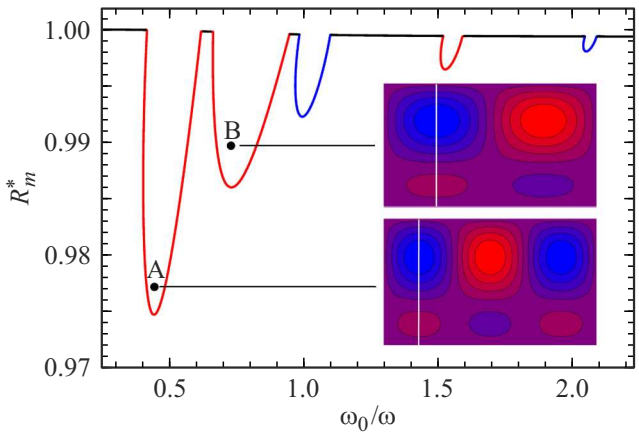

Figure 3. Dependence of the critical magnetic Rayleigh number R_m^* on the reduced inverse frequency of external modulation ω_0/ω. $\xi = 2$. Red line corresponds to subharmonic response, blue line corresponds to synchronous response, black line corresponds to quasiperiodic response. Insets show flow function isolines in the $z(y)$ plane: A — mode „32“ (described by the basis function with $n = 3, m = 2$) at $t = 4930$, B — mode „22“ at $t = 4925$.

shows thresholds corresponding to subharmonic response: $\gamma_1 = -1$. In case of $\gamma_1 = 1$, we have a synchronous system response boundary (blue line). Black line corresponds to quasiperiodic disturbances.

Position of all minima, except for the second one, in Figure 3 agrees with the rule of natural and external frequency ratio, which is standard for parametric problems [16]:

$$\omega_0/\omega = n/2, \qquad n = 1, 2, 3\ldots$$

Subharmonic response is characterized by half-integral frequency ratio. With synchronous response, natural frequency is a multiple of external frequency. Finally, the frequency ratio for quasiperiodic disturbances is irrational. On all curve segments, except for the second minimum, mode „32“, corresponding to the third horizontal harmonic $n = 3$ and second vertical harmonic $m = 2$ („six-roll“ flow) is implemented. Vertical asymmetry of rolls is associated with the fact that magnetic force is directed from the center to the narrow boundaries of the cell. Thus, in one half of the cell with $z > 0$ temperature gradient is co-directional with the magnetic field gradient — magnetic force forms instable fluid stratification. Consequently, in the other half of the layer, where temperature and magnetic field gradients are oppositely directed, stable stratification occurs. Thus, convective flow arising in a more heated region penetrates into an area near the cold boundary, but with a much lower intensity.

Expression (9) is violated for the second minimum, where the frequency ratio is different: $\omega_0/\omega \approx 3/4$. But, judging by the magnitude of the Floquet multiplier with the largest absolute value ($\gamma_1 = -1$), this minimum contains a subharmonic response. At first sight, parametric resonance laws are violated here. But the case is that another space mode

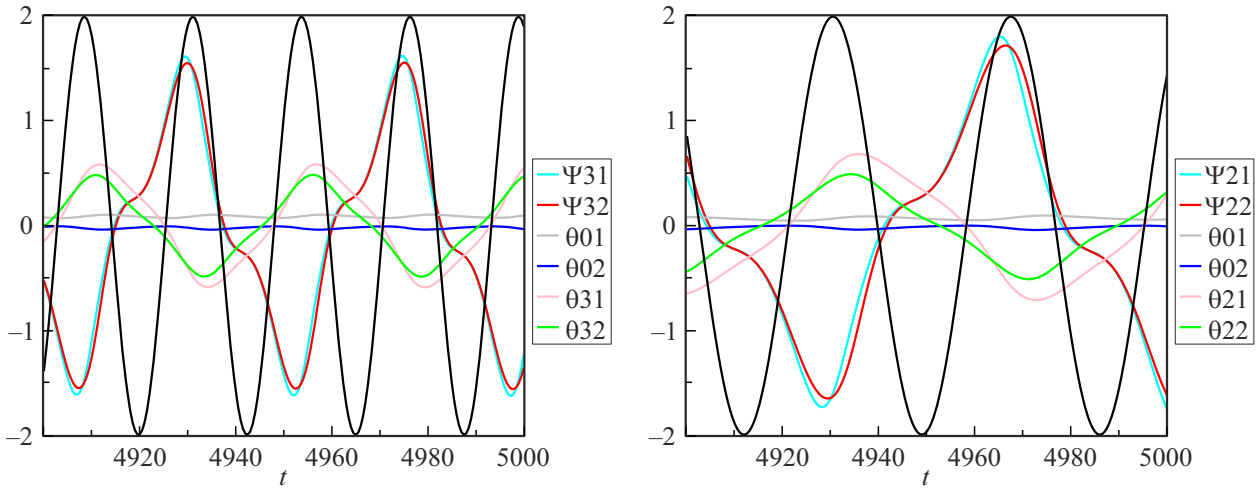

Figure 4. Diagrams of flow function amplitude evolution for six-roll (left) and four-roll (right) modes. Black line corresponds to external magnetic field oscillations. Numbers after Ψ and θ in the legend refer to n and m of the corresponding basis functions. For example, line $\theta 31$ describes evolution of the basis function of temperature with $n = 3$, $m = 1$.

„22“ („four-roll“ flow) is excited in the second minimum ($\omega_0/\omega \approx 3/4$). Generally speaking, for a constant magnetic field [10], instability boundary is associated with the „four-roll“ flow (vibrational mode „32“, $R_m^*(32) = 0.495$), and the monotonic „four-roll“ flow threshold (mode „22“) is located higher. ($R_m^*(22) = 0.54$).

Figure 4 shows flow function amplitude evolution and temperature curves for different space modes. Harmonic amplitude oscillations observed for the constant magnetic field [10] are somehow distorted by the external modulation. Six-wave flow at point ($R_m = 0.4837$, $\omega_0/\omega \approx 0.45$) and also marked in Figure 3 corresponds to the left curve, four-roll instability at point ($R_m = 0.4899$, $\omega_0/\omega \approx 0.73$) corresponds to the right curve. It can be seen that natural frequencies of these modes are different: $\omega_{01} \approx 0.123$ and $\omega_{02} \approx 0.085$, respectively. At the same time, both modes are a subharmonic response because the frequencies of all basis modes are lower than those of the external field. Thus, relation (9) isn't actually violated — the curve in Figure 3 is normalized to ω_{01}, which is not a natural frequency for the minimum in the $\omega_0/\omega \approx 3/4$ region. This minimum itself is induced by the parametric resonance excitation of four-roll space mode „22“ which was less dangerous for convection excitation in the constant field.

To clarify the nonlinear flow behavior, we analyze the system oscillations using the curve of $z_{\max}$ vs. time (Figure 5), for example, on line $y = 10$ for the four-roll mode and on line $y = 7$ for the six-roll mode (inset in Figure 3). For convenience, a dashed line in the figure additionally shows the variation of the alternating component of the external magnetic field with time. At $t = 4900$ (left curve), the flow function maximum is in the cell half characterized by negative coordinates z and retains its position during approximately a half of exposure period. A convective roll rotating clockwise correspond to these data and its amplitude smoothly increases from zero to maximum and then again decreases to zero. General flow structure corresponds to Inset A in Figure 3. Then the position of the flow function maximum (the roll rotating clockwise) moves to the upper third of the cavity. This means that rotation direction of rolls arranged vertically has changed. This flow structure is preserved during the next half of period and then returns to its initial position. Note that the $z_{\max}$ coordinate of maximum on each half-period is not strictly constant, but slightly varies, i.e. the global flow is a mixed state: a combination of a standing and running waves. Moreover, comparison of Figures 4 and 5 shows that when stable positions of the amplitude maximum ($t \approx 4938$ and ≈ 4983 on the left curves) of basis functions, which are the main one for a particular mode, velocities tend to zero allowing the modes with low amplitudes to form the flow structure.

Dependence of the stability threshold in the minima regions on the external alternating magnetic field amplitude (Figure 6) is discussed below. Threshold in the first minimum characterized by a subharmonic response decreases as a linear function as the amplitude grows. Critical numbers in the minimum region at $\omega_0/\omega \approx 1$ (synchronous response) decrease as a power function as the oscillation amplitude decreases. At the same time, the second tongue minimum ($\omega_0/\omega \approx 3/4$) occurs only when the critical amplitude $\xi^* = 0.96$ is reached. At $\xi < 0.96$, stability thresholds in this region are almost independent on the amplitude — quasiperiodic disturbance is observed. At $\xi > \xi^*$ critical numbers start decreasing as a linear function, subharmonic response is implemented. Figure 7 shows comparison of curves $R_m^*(\omega_0/\omega)$ for two cases: small $\xi < \xi^*$ (left) and large $\xi > \xi^*$ (right) exposure amplitudes. In the first case, only mode „32“ is excited and the curve fully meets the parametric resonance law (9), in the second case (with large exposure amplitude) competition between various space modes occurs: „32“ and „22“.

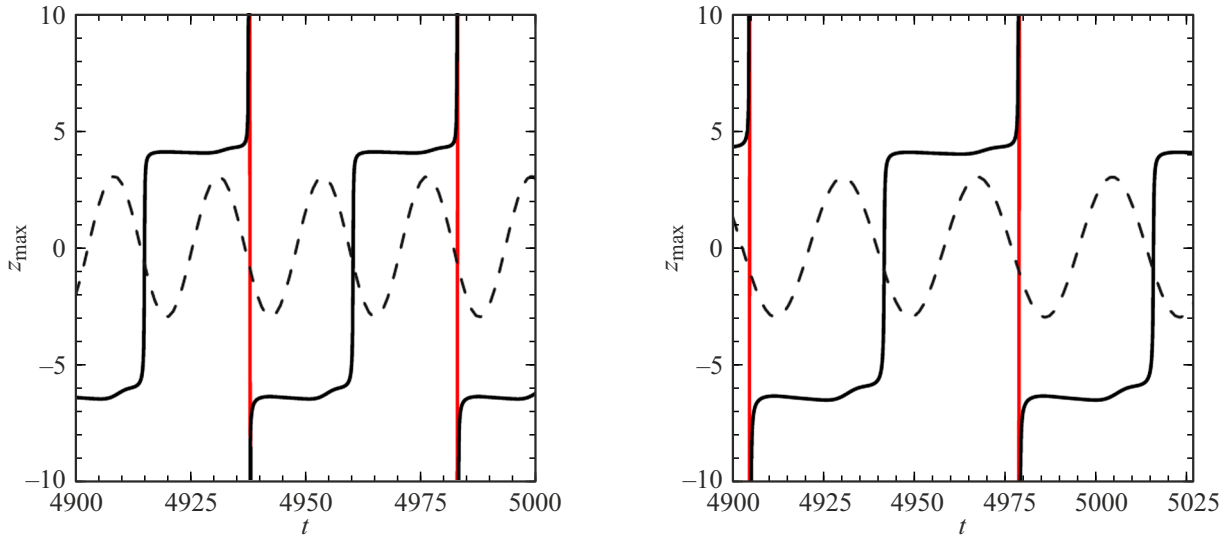

Figure 5. Dependence of the flow function maximum coordinate $z_{\max}$ on time at $R_m = 0.4837$, $\omega_0/\omega \approx 0.45$ (left) and $R_m = 0.4899$, $\omega_0/\omega \approx 0.73$ (right). Dashed lines — external modulation oscillation phase.

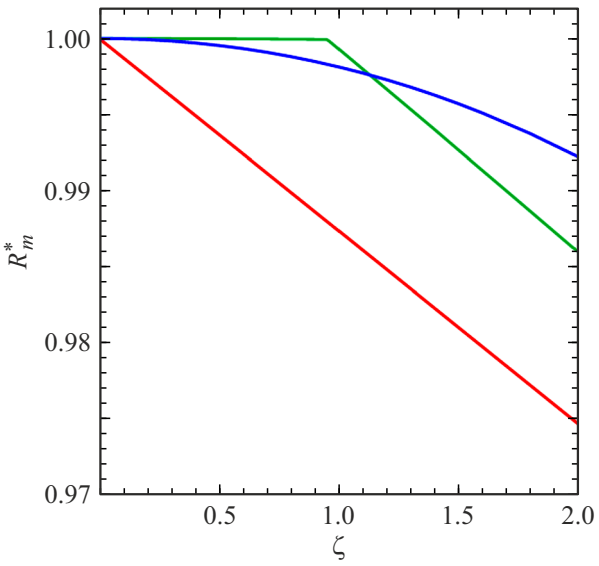

Figure 6. Dependence of the critical magnetic Rayleigh number R_m^* on the magnetic field modulation amplitude ξ in minima at $\omega_0/\omega \approx 1/2$ (red line), $\omega_0/\omega \approx 3/4$ (green line) and $\omega_0/\omega \approx 1$ (blue line).

Evaluate the characteristic values of quantities corresponding to oscillatory convection for the parametric resonance in the first minimum. For FF stratified by a concentration profile with $R_c = (\gamma^2/3) \cdot \alpha = 0.9$ and $\psi = 6$, which is exposed to an alternating field with dimensionless amplitude $\xi = 2$ and frequency $\omega = 0.278$ (Figure 3), a subharmonic response with the minimum critical magnetic Rayleigh number R_m^* equal to 0.4825 is observed, and the dimensionless period of an emerging oscillatory mode (response) is $\mathcal{T} = 45.2$. For experimental verification of theory, it is proposed to use the Hele–Shaw cell with $2d = 0.6$ mm and $h = 6$ mm and water-based magnetite (Fe_3O_4) ferrofluid with a particle diameter $a = 10$ nm and bulk magnetization $M_s = 480$ Gs. Magnetic moment m of the nanoparticle is equal to $2.51 \cdot 10^{-16}$ erg/Oe. For ferrofluid with $\varphi = 2\,\%$ and heated to the mean temperature $T_* = 300$ K, susceptibility is $\chi_* = 0.02$. When using $SmCo_5$ ($M_r = 600$ G) ring magnets with inside and outside radii $R_1 = 3$ cm and $R_2 = 5$ cm, respectively, and ring thickness $\mathcal{L} = 1.86$ cm, a constant magnetic field with the gradient $G \approx 107$ Oe/cm will be induced within the cell. In these conditions, the dimensionless alternating filed amplitude $\xi = 2$ of the Helmholtz coils corresponds to a dimensional value $A = \xi G d = 2 \cdot 107 \cdot 0.03$ Oe ≈ 6.42 Oe. Then for the cell with our ferrofluid sample we get $\gamma = mGh/k_B T_* = 0.386$, and the auxiliary set of parameters included in R_c and R_m is $\alpha = \chi_* G^2 d^4/\kappa\eta = 18$. Thus, it follows from $R_m = (\Delta T/T_*) \cdot \alpha$ that such thermomagnetic instability can be excited using $\Delta T = R_m T_*/\alpha = 0.4825 \cdot 300/18 \approx 8$ K. Dimensional oscillation period in this case will be

$$\mathcal{T}_{\text{dim}} = \mathcal{T} \cdot d^2/\kappa = 45.2 \cdot (0.03)^2/10^{-3} \approx 41 \text{ s}.$$

Conclusion

Parametric thermomagnetic convection of nonuniformly graded FF via thermodiffusion and magnetophoresis of magnetic nanoparticles has been investigated. FF fills the Hele–Shaw cell heated on the side of one of the narrow faces and placed into an alternating magnetic field. For different alternating magnetic field amplitudes, parametric instability characteristics were obtained: dependence of the critical magnetic Rayleigh numbers on the inverse frequency of neutral oscillations.

Characteristic flow function distributions are provided for supercritical oscillatory convection modes (within the first

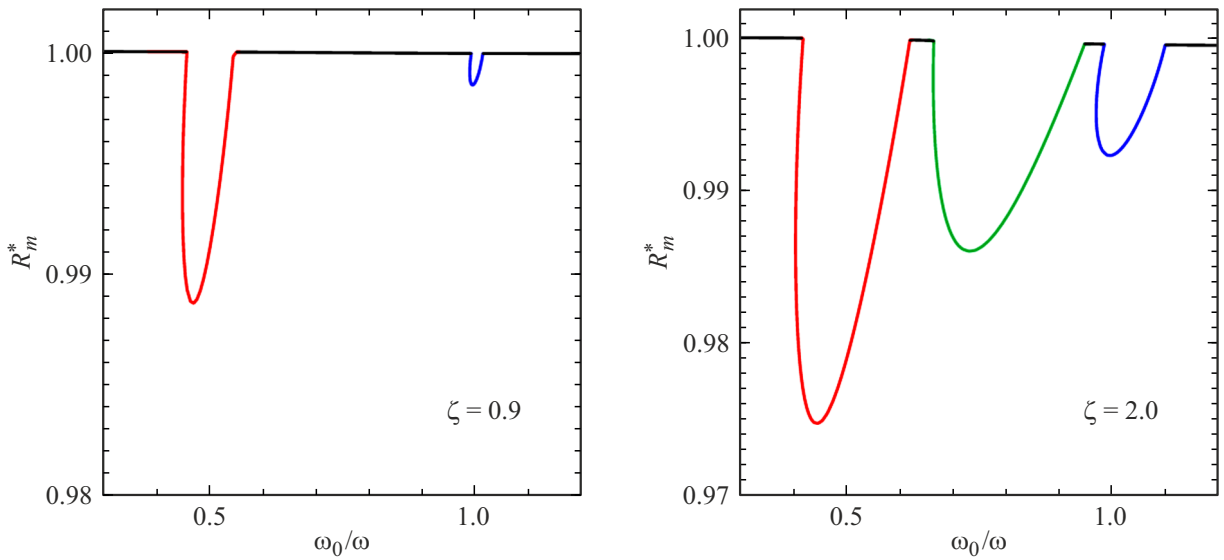

Figure 7. Dependence of the stability threshold on the natural and external frequency ratio for $\xi = 0.9$ (left) and $\xi = 2$ (right). Critical magnetic Rayleigh numbers are assigned to the maximum value on each of the curves.

and second parametric instability tongues), and amplitude-time behavior of various space harmonics is analyzed. It is shown that nonlinear FF flow is a „mixed" state; a standing wave with a small admixture of a running wave is implemented during the most part of the exposure period.

Conflict of interest

The authors declare no conflict of interest.

References

[1] M.I. Shliomis. Sov. Phys. Usp., **17** (2), 153 (1974). DOI: 10.1070/PU1974v017n02ABEH004332
[2] R. Rozentsvejg. *Ferrogidrodinamika* (Mir, M., 1989) (in Russian)
[3] B.M.Berkovsky, V.F.Medvedev, M.S.Krakov *Magnitnye zhidkosti* (Khimiya, M., 1989) (in Russian)
[4] B.A. Finlayson. J. Fluid Mechanics, **40** (4), 753 (1970). DOI: 10.1017/S0022112070000423
[5] P.J. Stiles, M. Kagan. J. Magn. Magn. Mater., **85**, 196 (1990). DOI: 10.1016/0304-8853(90)90050-Z
[6] A.A. Bozhko, S.A. Suslov. *Convection in Ferro-Nanofluids: Experiments and Theory* (Springer, Cham, 2018)
[7] P.V. Krauzin, P.N. Kazantsev, M.T. Krauzina. Microgravity Sci. Technol., **34** (5), 95 (2022). DOI: 10.1007/s12217-022-10010-3
[8] M.I. Shliomis, B.L. Smorodin. J. Magn. Magn. Mater., **252** (1), 197 (2002). DOI: 10.1016/S0304-8853(02)00712-6
[9] M.I. Shliomis, B.L. Smorodin, S. Kamiyama. Philosophical Magazine, **83**, 2139 (2003). DOI: 10.1080/0141861031000107908
[10] P.N.Kazantsev, B.L.Smorodin. PMTF, **66** (2), 129 (2024). DOI: 10.15372/PMTF202415534
[11] G.Z.Gershuni, I.O.Keller, B.L.Smorodin. Dokl. RAS, **348** (2), 194 (1996).
[12] V.G.Kozlov, S.V.Subbotin. PMTF, **59** (1), 28 (2018). DOI: 10.15372/PMTF20180104
[13] V.A. Il'in, B.L. Smorodin. Tech. Phys. Lett., **31** (5), 432 (2005). DOI: 10.1134/1.1931790
[14] N.N. Kartavykh, B.L. Smorodin, V.A. Il'in. J. Experimental and Theoretical Physics, **121** (1), 155 (2015). DOI: 10.1134/S1063776115080087
[15] L.D. Landau, E.M. Lifshits. *Mekhanika* (Fizmatlit, M., 2004) (in Russian)
[16] M.I.Rabinovich, D.I.Trubetskov. *Vvedeniye v teoriyu kolebaniy i voln* (Nauka, M., 1994) (in Russian).
[17] H. Lamb. *Hydrodynamics* (Univ. Press, Cambridge, 1993)
[18] A.F. Pshenichnikov. Magnetohydrodynamics, **29**, 33 (1993).
[19] L.D. Landau, Ye.M. Lifshits. *Gidrodinamika* (Fizmatlit, M., 1986) (in Russian)
[20] D.V.Lyubimov, E.M.Putib, V.I.Tchernatynsky. DAN SSSR, **235** (3), 554 (1977).
[21] L.V.Kantorovich, V.I.Krylov. *Priblizhennye metody vysshego analiza* (Fizmatgiz, L., 1962) (in Russian)
[22] E.A. Coddington, N. Levinson. *Theory of ordinary differential equations* (McGraw-Hill, NY., 1955)
[23] J.H. Wilkinson, C. Reinsch. *Handbook for Automatic Computation, Linear Algebra* (Springer, Berlin, 1971)

Translated by E.Ilyinskaya